Egypt. J. Rad. Sci. Applic. **Vol. 37,** No.1-2 pp. 39 - 54 (2024)

Egyptian Journal of Radiation Sciences and Applications
http://ejrsa.journals.ekb.eg/

Preparation and Modification of Ethylene Vinyl Acetate (EVA)/ Rosin Blends with Gamma Radiation for Antimicrobial Applications

M. M. Magida[1]*, Faten Ismail Abou El Fadl[2], Eman Araby[3], Sayeda M. Ibrahim[1]
[1]Department of Radiation chemistry, National Center for Radiation Research and Technology (NCRRT), Egyptian Atomic Energy Authority (EAEA), [2]Department of Polymer chemistry, National Center for Radiation Research and Technology (NCRRT), Egyptian Atomic Energy Authority (EAEA),[3] Department of Radiation Microbiology, National Center for Radiation Research and Technology (NCRRT), Egyptian Atomic Energy Authority (EAEA), Cairo, Egypt.

BLENDS of Ethylene-vinyl acetate and rosin EVA/Rosin with different ratios have been prepared by solution casting technique followed by exposure to different doses of gamma radiation. The blends (EVA/Rosin) were characterized by FTIR, scanning electron microscopy (SEM), X-Ray Diffraction (XRD) and mechanical properties. The blend films show noticeable miscibility between EVA and rosin at higher concentration of EVA specially 75% EVA and 25% Rosin proved by FTIR and SEM. XRD studies show that the crystallinity and phase behavior of EVA/Rosin blends varied with different ratios of the two components. It was also established that the mechanical properties were enriched with the addition of EVA to rosin. After that, the EVA/Rosin blends were modified through incorporation of silver nanoparticles (Ag NPs) and cinnamic acid (Cinn) with gamma radiation. Antimicrobial and antibiofilm efficiency of all films were assessed against Staphylococcus aureus (S. aureus), Pseudomonas aeruginosa (P. aeruginosa), and Candida albicans (C. albicans). The antimicrobial results had generally indicated that the all films showed a deactivation order to all the studied microbes. In a remarkable result, EVA/Rosin/ (Cinn/Ag) 5% had the most potent influence against all the examined strains. Furthermore, the synthesized compounds demonstrated improved qualitative and quantitative biofilm repression for all the tested strains. The SEM analysis of the treated cells showed noticeable morphological abnormalities (the complete lysis of the outer surface followed by deformations of cells with a rough and irregular surface). Accordingly, synthesized nanocomposites open the area of interest for environmental and biomedical applications.

Keywords: ethylene-vinyl acetate, rosin, antimicrobial activity, ionizing radiation.

Introduction

Blending of polymers is a common technique and simple practice method applied in industry in order to achieve improved final product properties to design a completely new polymeric material [1]. Ethylene vinyl acetate and rosin (EVA)/ Rosin blends are versatile materials with diverse applications across industries. Commonly used in adhesives, these blends offer strong bonding capabilities suitable for packaging, woodworking, and shoe manufacturing. They are also integrated in hot melt adhesives, providing excellent adhesion to materials such as plastics, wood, and metal in automotive and electronics industries.[2, 3]. Additionally, their formulation extends to sealants, coatings, and printing inks, where they offer properties such as weather resistance, flexibility, and printability on various substrates. EVA/Rosin blends have gained attention for their potential antimicrobial applications due to the inherent properties of both EVA and rosin. To prepare these blends, EVA and rosin are first mixed in appropriate ratios to achieve the desired properties.

**correspond author email: magida-ahmed@hotmail.com*
Received 19 / 3 / 2024 ; Accepted 12 / 5 / 2024
DOI: 10.21608/EJRSA.2024.277944.1167

The blending process can be tailored to optimize characteristics such as mechanical strength, flexibility, and antimicrobial activity. Gamma radiation effectively modifies the molecular structure of the polymer, enhancing its antimicrobial properties. This is achieved through the generation of free radicals and subsequent crosslinking or chain scission reactions within the polymer matrix. The reduction process under gamma irradiation is rapid and efficient, leading to the formation of AgNPs with narrow size distribution.

The antimicrobial efficacy of the EVA/Rosin blend can be further enhanced by adjusting the radiation dosage and conditions. Higher doses of gamma radiation can lead to increased crosslinking density, thereby improving the material's resistance to microbial growth. Additionally, the introduction of specific additives or antimicrobial agents such as AgNPs nanoparticles and cinnamic acid during the blending process can synergistically enhance the antimicrobial activity of the material. A natural aromatic carboxylic acid, cinnamic acid, is a key chemical component found in plants including Cinnamomum cassia, Chinese cinnamon, Panax ginseng, whole grains, fruits, vegetables, and honey [4] .The existence of an acrylic acid group substituted on the phenyl ring gives cinnamic either a cis or a trans configuration with the latter being the most common of the two. When microorganisms adhere to a surface and/ or to each other, microbial growth is known as biofilm. Biofilms are inhabitants of multilayered cells that grow on a surface and are enclosed in an exopolysaccharide matrix (EPS) and cause antimicrobial resistance due to the adherence of microorganisms to biotic surfaces like host cells or abiotic surfaces like medical devices. The formation and development of biofilm are affected by surface proteins and polysaccharide intercellular adhesions (PIA). Biofilm-embedded bacteria are challenging to treat (Kırmusaoğlu 2016) [5] .

Silver nanoparticles (Ag-NPs) are among the most favored metal NPs due to the multiple functionality as pronounced antimicrobial agent[6-8]. Ag-NPs has been explored widely and used in various industrial applications and incorporated into a variety of household and consumer products including textiles, cosmetics, paints, coatings, sensor, agricultural and food packaging, with a relatively high usage compared to other metals and alkaline earth metals in NPs applications[9]. Ag-NPs can be synthesized by different techniques, such as evaporation-condensation[10], laser ablation[11], gamma irradiation[12], lithography[13], microwave-assisted technique[14] and biosynthesis using plants[15]. Generally, three different methods of synthesis used are physical, chemical, and biological method [16, 17].

Gamma (γ) irradiation is a mature and powerful technology to be considered for the synthesis of Ag-NPs. Irradiation technique is considered a "green technique" as it does not require chemical initiator for reduction unlike the conventional methods[18]. It is a simple, clean process which cans be performed using aqueous system, at ambient pressure and room temperature. The reduction of metal NPs by γ-irradiation is controlled by the dose of irradiation while the NPs produced are very pure fully reduced without tracing of chemicals[19].

The combination of AgNPs and cinnamic acid with the EVA/Rosin blend offers a synergistic effect, resulting in increased antimicrobial efficacy. The presence of these additives not only inhibits microbial growth, but also prolongs the material's antimicrobial activity over time. Overall, the addition of AgNPs and cinnamic acid to the EVA/Rosin blend, along with gamma radiation modification, presents a comprehensive approach to developing antimicrobial materials suitable for a wide range of applications, from healthcare to food packaging.

The present study focused on the preparation and characterization of un-irradiated and gamma-irradiated various compositions of (EVA/rosin) blends modified through the incorporation of silver nanoparticles Ag NPs and cinnamic acid Cinn into EVA/Rosin separately or in combination. In this regard, the objective of this study is to evaluate the antimicrobial and antibiofilm effects of four of the tested compounds: EVA/Rosin; EVA/ Rosin/Cinn5%; EVA/Rosin/ Ag NPs5%; and EVA/Rosin/ (Cinn/ Ag NPs) 5% synthesized by gamma-irradiation to evaluate the antimicrobial and antibiofilm effects against some pathogenic strains.

Experimental

Materials

EVA copolymer-18% aromatic compound, MFI 135g/10min, melting point 67°C was obtained from ArkemaInc, USA. Rosin was obtained from HAB. Co, India. Cinnamic acid, Ag NO_3 was purchased from Sigma-Aldrich Co. Germany. The

structures of EVA and rosin are illustrated in Fig. 1. A pure grade of methylene chloride obtained from MACRON Fine Chemicals, Poland was used in the preparation of EVA/ Rosin blends. This solvent was chosen since a single phase of blends can be obtained.

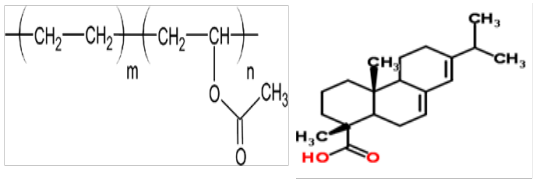

a) **b)**

Fig. 1. The structure of a) Ethylene vinyl acetate (EVA) and b) Rosin.

Preparation of EVA /Rosin Blends

Blends of EVA/Rosin were prepared by casting solution technique. Solutions of EVA and rosin in methylene chloride solvent were prepared at various compositions: (25/75, 50/50. 75/25) EVA/ Rosin (wt/wt %). Then the solutions subsequently cast onto Petri dishes to form transparent films and then were dried under ambient conditions for 24 hours. All films were subjected to gamma irradiation at various doses (20, 50, 100 and 200 kGy) of gamma radiation.

Preparation of pure Silver NPs and Cinnamic acid/Silver (Cinn/AgNPs)

Firstly, 100 ml of Cinnamic acid (0.5% w/v) prepared by dissolving 0.5 g in 100 ml distilled water and $AgNO_3$ solution of 0.5 M were prepared, secondly, 100 ml of cinnamic acid was added to 100 ml of $AgNO_3$ solution (0.5M) in a 250 ml beaker coated with aluminum foil then this mixture and 100 ml of silver nitrate solution (0.5M) with, separately, then exposed to gamma radiation at 20 kGy to enhance the reduction of Ag^+ ions to Ag NPs. When irradiation is applied to metal ions in an aqueous solution, irradiation energy is absorbed in water, which causes radiolysis of water and several products are generated, including hydrated electrons ($e_{aq}-$), radical hydrogen atoms (H•) and radical hydroxyl (OH•) which are dispersed uniformly in the reaction medium (Eq. 1)[20]. The radiolytic method via γ-radiation is a powerful technique which can produce the desired morphology and distribution of metal NCs by adjusting the dose of irradiation[21]. In the aqueous solution, $AgNO_3$ separates to Ag+ and NO_3 − ions as shown in Eq. 2. The powerful reductant generated from the radiolytic process, such as active electrons e_{aq} − and H atoms (H•),

$$n*H_2O \xrightarrow{\text{irradiation}} e^{\cdot}_{aq} + OH\bullet + H\bullet \quad (1)$$

$$AgNO_3 \longrightarrow Ag^+ + NO_3^- \quad (2)$$

$$Ag^+ + e^-_{aq} \xrightarrow{\text{reduction}} Ag^0 \quad (3)$$

$$Ag^+ + H\bullet \longrightarrow Ag^0 + H^+ \quad (4)$$

will reduce silver ions (Ag+) to the zerovalent state (Ag^0) (Eqs. 3-4).

The reduced neutral silver atom Ag^0 tends to interact with other metal ions to form relatively stable Ag clusters which combines with neighboring silver atoms and progressively grew into large clusters to form spherical Ag-NCs [22,23]as follows (Eqs. 5-8):

$$Ag^0 + Ag^+ \rightarrow Ag^{2+\bullet} \quad (5)$$

$$Ag^{2+\bullet} + Ag^+ \rightarrow Ag_3^{2+\bullet} \quad (6)$$

$$Ag_2^{+\bullet} + Ag_2^{+\bullet} \rightarrow Ag_4^{2+} \quad (7)$$

$$(Ag)_n^+ + ne^{\cdot}_{aq}\, n^{\cdot} \rightarrow (Ag)_n \quad (8)$$

Both Nano dispersions Cinn/ AgNPs and pure AgNPs nanoparticles were centrifuged at 6000 rpm for 10 min. The powders were separated from the supernatant, washed using deionized water, dried at room temperature, and kept at room temperature in a separate sealed glass bottles.

Preparation of EVA/ Rosin nanocomposite films

Films of EVA/ Rosin/Ag5%, EVA/ Rosin/Cinn 5% and EVA/ Rosin/ (Cinn/Ag) 5% nano composite films were obtained by adding powder of Ag NPs, Cinn and Cinn/ AgNPs to EVA/ Rosin blend during preparation through stirring until complete miscibility. All films were subjected to gamma irradiation at various doses (20, 50, 100, and 200 kGy) then cut into pieces for various measurements.

Gamma irradiation

Gamma irradiation of fabricated samples was carried out by the Cobalt-60 source of Gamma Chamber-4000A, fabricated by Atomic Research Center- India, introduced at the National Center for Radiation Research and technology, Cairo, Egypt. The composites were subjected to gamma irradiation in the air at room temperature at a measurements rate of ≈ 1.11 kGy/h.

Characterization Techniques
FTIR spectroscopic analysis

For FTIR measurements, Vertex 70 Fourier Transform Infrared spectrophotometer from Bruker, Germany was used.

Scanning electron microscope (SEM)

Scanning electron microscopy (SEM) (Jeol, JSM) examined the surface of the samples at a voltage of 30 kV. In order to reduce charging in the SEM, the surfaces were precoated with a thin gold layer

Transmitting electron microscopy (TEM)

A dispersion of the nanoparticles suspended in water, was deposited on an ultra-thin carbon supported Cu grid, and air-dried. Then the particle size and shape were evaluated using TEM JEOL: JEM-100cx.

XRD Diffraction

XRD by Shimadzu apparatus examined the prepared copolymer blend EVA/Rosin using nickel filter, copper K target, voltage =40 (kV), current = 30 (mA), and scan speed = 8 (deg min^{-1}) (Shimadzu Scientific Instruments (SSI), Kyoto, Japan).

Mechanical Properties

Mechanical tests tensile strength(Ts) and elongation at break% (Eb%) for all blend compositions were performed on the triplets at room temperature using a Mecmesin, model 10-I, UK, with a crosshead speed of 500 mm/min.

Microbiological Studies
Evaluation of Antimicrobial Activity

Four compounds used in this experiment: 1. EVA/Rosin (E/R) blank, 2. EVA/Rosin/Cinnamic acid (E/R/C 5%), 3. EVA/Rosin/ Ag NPs (E/R/ AgNPs5%), and 4. EVA /Rosin/Cinnamic acid/ Ag NPs (E/R/C/AgNPs 5%).

Microbial Cultures

At the Microbiology Department, NCRRT, Staphylococcus *aureus (S. aureus*), *Pseudomonas aeruginosa (P. aeruginosa),* and *Candida albicans (C. albicans)* were previously isolated and characterized as representatives of (Gram positive), (Gram-negative) bacteria and unicellular fungi, respectively. *S. aureus* and *P. aeruginosa* were cultivated on nutrient agar (NA) plates, while *C. albicans* was grown on Sabouraud-Dextrose agar (SDA). All cultures were kept in agar slants at a temperature of 4 °C.

Total plate count (quantitative measurement)

According to the AATCC Test Method (1961), 24 the quantitative assessment of the antimicrobial activity of the tested compounds was evaluated. The tested compound discs were inserted into a sterile screw-capped tube containing nutrient broth medium (NB). 100 µl of 10^6 CFU/ml from the different tested strains was loaded on each tube with an even distribution of the inoculate. 10-fold dilutions in sterile saline solution were prepared following 18 h. incubation at 32°C. 100 µl from each dilution was surface inoculated on NA plates and incubated aerobically at 32 ◦C for 18 h. Colony-forming units (CFU/ml) are used to measure and express the number of colonies obtained. Three duplicates of the experiment were run.

Qualitative determination of slime production
Congo red agar (CRA) technique

Freeman et al. (1989)[25] established a simple qualitative method to determine slime production using Congo Red Agar (CRA) medium. Brain heart infusion broth medium (Oxoid, UK) containing (50 g/L of sucrose, 10 g/L of agar No. 1, and 0.8 g/L of Congo red indicator) were prepared to make the CRA medium. Initially, a concentrated aqueous solution of Congo red stain was prepared, and it was autoclaved (at 121°C for 15 minutes) separately from the other ingredients of the medium. Then with sucrose at 55°C, it was mixed with the autoclaved brain heart infusion agar. The tested strains were inoculated onto Congo red agar plates (untreated and treated with the examined compounds), and incubated at 37°C for 24 h. Biofilm formation was characterized by black colonies with a dry, crystalline consistency. The experiment was carried out in triplicate.

Anti- biofilm activity of the tested compounds

This quantitative test described by Christensen et al. (1985)[26] is considered the gold-standard method for biofilm detection (Gupta et al., 2019).[27] Observations of the bacterial and yeast biofilm formed on the test tubes' interior walls were obtained both with and without the investigated compounds. In comparison to control samples (test tubes without any treatment), the antibiofilm activity of the E/R, E/R/C 5%, E/R/Ag NPs 5%, and E/R/C/Ag NPs 5% was assessed against the studied strains. A loopful of test organisms was inoculated in 10 mL of trypticase soy broth with 1% glucose in test tubes, and the tubes incubated for 24 h. at 37 °C. After incubation, the tubes were decanted, washed with phosphate buffered saline (pH 7.3), and dried. After that, tubes were dyed with crystal violet (0.1%). Deionized water is used to remove extra stains. Tubes dried in an inverted position. According to the findings of the control strains, the scoring for the tube technique was performed. A visible film that lined the tube's bottom and wall was a sign that a biofilm was forming successfully. The amount of biofilm formed was scored as 1-weak/none, 2-moderate, and 3-high/strong. Using a Microplate Reader-Suno Stick SPR-960B at 595 nm, the optical densities (ODs) of the stained adherent biofilms were measured in order to detect the microbial biofilm quantitatively. The experiments were carried out in triplicate.

Scanning electron microscopy

Scanning electron microscopy (SEM) examinations on the tested bacterial strains were performed in order to determine and elucidate the morphological changes in bacterial cells cultivated with EVA/Rosin/(Cinn/Ag NPs) 5% for 18h. incubation period. Before and after treatment, cells of *S. aureus* and *P. aeruginosa* were fixed with 2.5 % glutaraldehyde for an overnight period, buffered with 0.1M sodium phosphate buffer (pH 7.2) for an hour at room temperature, washed four times in sodium phosphate buffer, and then post-fixed with 1% osmium tetroxide in the same buffer for another hour, followed by another wash in the same buffer. After that, they underwent a graded alcohol dehydration process (30, 50, 70, 90, and 100%). Following an overnight drying process, SEM analysis was performed on each sample. The SEM micrographs were taken with a JSM-5400 instrument by JEOL-Japan.

Results and discussions

FTIR Spectroscopy

FTIR analysis of EVA/Rosin blends with varying ratios reveals distinct spectral features that provide insights into their chemical composition and interactions. The FTIR spectra of pure EVA, pure rosin and their blend at a composition of EVA/rosin 75/25 before exposure to gamma radiation are presented in Fig. (1). Fig. (1) shows that blends display peaks from both EVA and rosin, indicating some degree of interaction or compatibility between the components. As can be seen, the characteristic bands of EVA (100%) are presented where the band at 2906 cm^{-1} is attributed to the stretching CH_2 group, the band at 1741 cm^{-1} is related to the C=O in the ester group in the vinyl acetate region, bands at 1251, 1031, and 792 cm^{-1} are due to symmetric and unsymmetrical C-O-C group. The IR spectrum of rosin 100% shows the absorption bands at 2872 and 2952 cm^{-1} assigned to methyl and methylene asymmetric and symmetric stretching vibrations. The band at 3344 cm^{-1} is due to the OH group of the carboxylic group of rosin. The absorption at 1695 cm^{-1} for rosin 1701 cm^{-1} is related to the C=O group and the bands in the region 1460-945 cm^{-1} are due to the aromatic ring. Careful examining of the IR spectrum of the EVA/rosin 75/25 blend resulted in combination and overlapping of the characteristic bands of both EVA and rosin with shift in wave number and decrease in the intensity of some bands due to interaction between EVA and Rosin where shifts in peak positions may suggest intermolecular interactions such as hydrogen bonding or dipole-dipole interactions. In the case of irradiated blend, the peaks at 2861 and 2925 cm^{-1} were attributed to the asymmetric and symmetric vibrations of stretching C–H in the pyranoid ring[28]. At 1692 cm^{-1}, the broad peak centers are associated with stretching C=O in both EVA and rosin. There is a good connection between these data depending on the fact that the gamma irradiation causes cross-linking of the EVA/ Rosin blend. At this point, the peaks at 1141, 1183, and 890 cm^{-1} are associated to the widening of the vibrations of the alkyl peroxides stretching (C–O–O–C), the vibration of the stretching (C–O) of carboxyl group, and out of plane bending vibration of $CH(CH_2{=}CH{-}H)$. Hence, the results obtained demonstrate that there is an increase in the methylene motion and cross-linking of molecules of the EVA/ Rosin blend which is induced by the gamma irradiation[29]. However, the gamma rays have the ability to be absorbed even by C–C and/or C–H bonds. Thus, formed radicals led to the formation of high amount of cross-links in blend of the EVA/ Rosin blend[30]. In general, FTIR results indicated the interactions between functional groups in EVA and Rosin in which FTIR analysis facilitates understanding the chemical changes occurring in EVA/Rosin blends, aiding in their characterization and optimization for various applications.

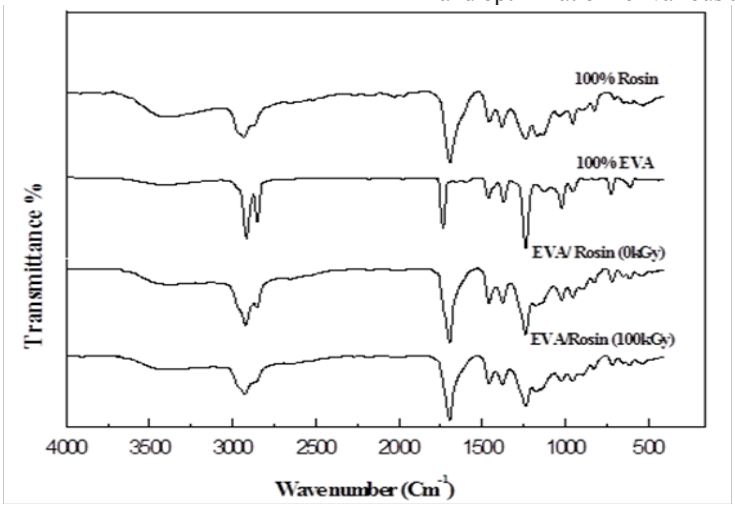

Fig. 1. FTIR spectra of unirradiated EVA, Rosin, unirradiated EVA/Rosin (75/25) blend and irradiated EVA/ Rosin (75/25) at 100 kGy.

Scanning Electron Microscope

Scanning Electron Microscope (SEM) imaging of EVA/Rosin blends provides visual information about the surface morphology and microstructure of the blends, offering valuable insights into their compatibility and phase distribution at the micro scale. Fig.s 2 (a-d) show the SEM images of EVA, Rosin, and both unirradiated and irradiated EVA/ rosin (75%/25 %) blend at 100kGy. The SEM pattern of unirradiated EVA is shown in Fig. 2a. The fracture surface of EVA is dense, tabular, and smooth, and no sign of porous structure is visible in the samples displaying a regular layered structure. In Fig. 2b, the SEM of the unirradiated rosin observed that the surface was rock shape, rough, and with sharp edges. Unirradiated polymeric blend containing EVA/ rosin shows rough surface, with holes. The EVA particles dispersion shows that a small interfacial tension exists between rosin particles. For this blend, small holes and a network of canals have appeared as shown in Fig. 2c. In Fig. 2d the image of the irradiated EVA/ rosin blends at 100 kGy shows a more homogenous structure compared to the unirradiated blend. The EVA content in the blend causes the formation of an interpenetrating polymer network and makes the samples more elastic. Irradiation changes the polymer network; therefore, it changes the morphological state of the polymer[31]. SEM images may reveal a more uniform distribution of both EVA and rosin phases with smaller and more evenly dispersed rosin particles within the EVA matrix where smooth continuous surface with an indication of increasing interfacial adhesion between the two phases, which suggests the formation of crosslinking, as shown in Fig. 2d. This may account for crosslinking and the disappearance of parting due to phase contraction. This suggests better compatibility between the two components, with potential interactions leading to a more homogeneous microstructure.

Meanwhile, it can be proved that the irradiation process increases the crosslinking degree of the blend, which modifies the interface of the blends and enhances the interaction of the two polymers. These findings indicate an improvement in the compatibility between EVA and Rosin polymer matrix.

XRD diffraction

X-ray diffraction (XRD) analysis is a powerful technique used to study the crystalline structure of materials, providing insights into their composition and properties. In the case of an Ethylene Vinyl Acetate (EVA)/Rosin blend, XRD can reveal information about the crystalline phases present and their distribution within the blend. Fig. (3) shows the XRD patterns of unirradiated, and irradiated EVA, rosin and EVA/ Rosin (75/25) blend. All samples exhibited a broad peak as in the case of rosin, a broad characteristic peak observed at 15.1^{o} reflecting the amorphous nature of rosin. The diffraction pattern of pure EVA denotes a diffraction peak of around 21.2° which represents its semicrystalline nature, caused by the presence of strong intramolecular hydrogen bonding in individual monomer units of EVA and intermolecular hydrogen bonding between its different monomer units. For unirradiated and irradiated EVA/ Rosin blend, there is a characteristic peak at 22.46^{o}. At lower Rosin content, the XRD pattern may primarily exhibit peaks corresponding to the crystalline phases of EVA, such as the peaks associated with its ethylene segments. As the Rosin content increases, additional peaks may appear, corresponding to the interactions between the two components. This suggests possible interactions between EVA and Rosin molecules leading to the formation of new crystalline structures or altering the existing ones. However, in the situation of unirradiated EVA/ Rosin, there was a high intensity in the peak at 22.46°. This could be used for revealing the presence of cross-linking structure of the irradiated blend[32]. Fig. 3. XRD of unirradiated and irradiated EVA, Rosin and EVA/Rosin (75/25) blend.

Mechanical Properties

The mechanical properties of Ethylene Vinyl Acetate (EVA)/Rosin blends, including tensile strength (Ts) and elongation at break (Eb %), are crucial factors in determining their suitability for various applications. Studies have investigated how these properties vary with different ratios of EVA and Rosin. Fig. (4a) illustrates the tensile strength (T_s) as a function of radiation dose of pure EVA and different concentrations of EVA/ Rosin blends. It can be observed that the tensile strength of pure EVA is significantly greater than the tensile strength of EVA/ Rosin blends. On the other hand, the tensile strength tended to decrease as the ratio of rosin increased in the blend. This reduction in tensile strength could be attributed to several factors, including the presence of less cohesive rosin phase, reducing the overall strength of the blend. The effect of gamma irradiation at 100 kGy on the mechanical properties of EVA/ Rosin blends with different ratios was studied. It was observed that irradiation caused changes in the molecular structure of the polymer blend, which in turn affected its mechanical behavior. Upon irradiation, the tensile strength of blends increased up to a dose of 100 kGy. It is obvious that the Ts values are correlated to EVA content. This may suggest the impact of the progressive chain crosslinking, taking place by radiation in the EVA content, on the overall blend Ts value. Generating high levels of free radicals for each irradiation were possible due to the presence of conjugated

π bonds inside the EVA chemical structure. These observations correspond to the increased crosslinking density of the blend samples. The latter value exhibited declination with the higher doses up to 100 kGy. The reductions expectedly caused by chain scission brought about by excessive doses. Fig. (4b) demonstrates variation in elongation at break% (E_b) with irradiation at various EVA ratios. In case of unirradiated EVA/ Rosin blend, the elongation at break (Eb%) showed a different trend. At higher EVA content, the Eb% increase where it typically exhibits high flexibility and elongation. However, as the EVA content increased, the Eb% might also increase due to the plasticizing effect of EVA, enhancing the flexibility and elongation of the blend. This effect is often observed in polymer blends where the presence of EVA increases the polymer chain mobility. On the other hand, in case of irradiated blends as the absorbed gamma dose increases, elongation at break decreases. The increased irradiation enhanced the three-dimensional gel-like structure inside the polymer blends, leading to a decreased internal chain mobility and elongation. Moreover, gamma irradiation can induce crosslinking, which may increase the blend's resistance to deformation and elongation at break. As the radiation dose increases more crosslinking is produced in the sample matrix preventing the structural reorganization during drawing[33]. Thus, the radiation crosslinking that occurs in the EVA content affirmed by the Eb% dependence on the blend composition.

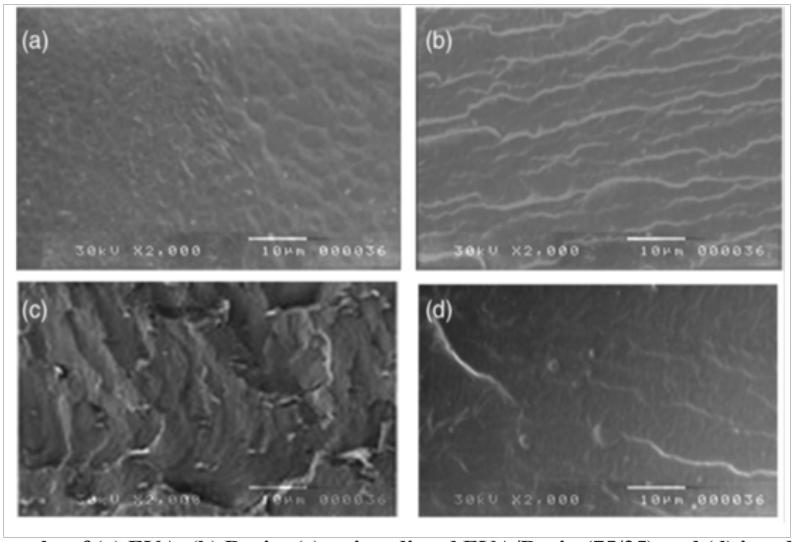

Fig. 2. SEM photographs of (a) EVA, (b) Rosin, (c) unirradiated EVA/Rosin (75/25),and (d) irradiated EVA/Rosin (75/25) at 100 kGy.

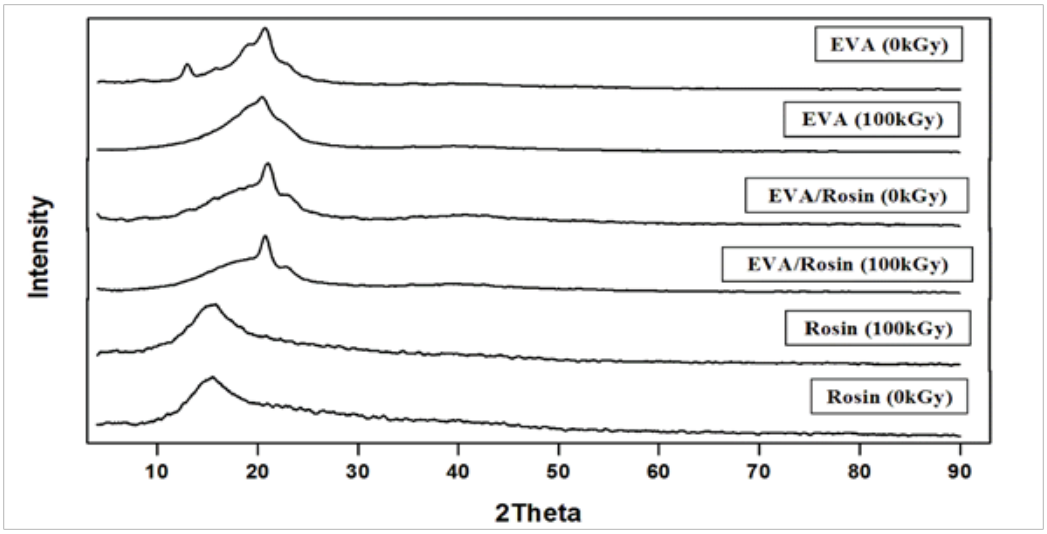

Fig. 3. XRD of unirradiated and irradiated EVA, Rosin and EVA/Rosin (75/25) blend.

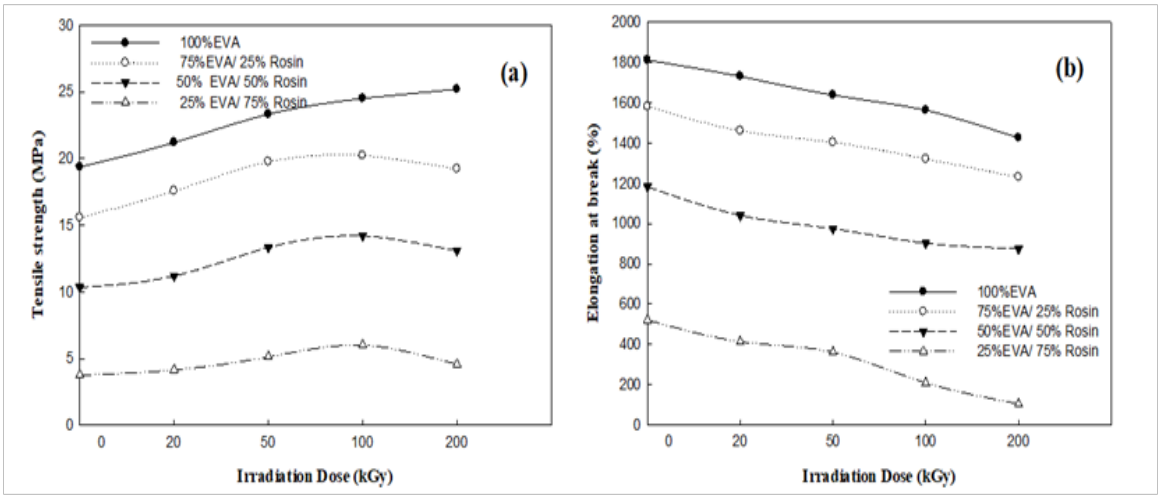

Fig. 4. Effect of irradiation dose on the a) Ts of EVA (100%) and its blends with Rosin at various compositions and b) Eb% of EVA (100%) and its blends with Rosin at various compositions.

Transmission Electron Microscope

TEM imaging of pure AgNPs and Cinn/ AgNPs offers a detailed understanding of their size, morphology, and surface characteristics. This information is crucial for optimizing synthesis protocols and understanding the potential applications of these nanoparticles in various fields such as catalysis, biomedicine, and sensing. Fig. (5) shows the TEM images for pure Ag NPs (5a) and Cinn/ Ag NPs (5 b). It is obvious from the Fig. the great change in the pure Ag NPs and its shape and size in the Cinn/ Ag NPs nanocomposite where the size of Ag NPs appear smaller than in case of Cinn/ Ag NPs nanocomposite. The coating of Ag NPs with Cinnamic acid has a great effect on the formed Ag NPs and causes its enlargement in its size due to the bulk size of cinnamic acid. The size of the pure Ag as estimated from the image was (10.2 nm) while after coating with Cinnamic became (13 nm).

X-Ray Diffraction (XRD)

X-Ray Diffraction (XRD) analysis provides valuable structural information about silver nanoparticles (AgNPs) and cinnamic acid (Cinn/ Ag NPs). Fig. (6) presents the XRD of the Cinn/ Ag NPs nanoparticles. It is obvious from the XRD patterns the combination of both patterns of cinnamic and silver nanoparticles reflecting potential alterations in the crystal structure or the presence of an organic coating. The diffraction peaks of Cinn/ AgNPs may show slight shifts or broadening due to the interaction between the cinnamic molecules and the surface of the AgNPs nanoparticles. Additionally, new peaks corresponding to the cinnamic molecule may be observed, indicating its successful attachment to the AgNPs nanoparticles. As it can be noticed from the Fig. the appearance of the characteristic peaks of AgNPs nanoparticles at 2- theta 17˚, 28˚, 38˚, 48˚ and 65˚, while the highest characteristic peaks for cinnamic acid is appeared at 2- Theta 12˚, 15˚, and 20˚.

Antimicrobial Assessment

Fig. (7) displays the antimicrobial activity of the four investigated compounds against *S. aureus, P. aeruginosa,* and *C. albicans,* which are, respectively, examples of (Gram-positive, Gram-negative) bacteria and fungi, by calculating and representing log10 colony-forming unit per milliliter. It is evident that throughout the 18-h. contact period with control and blank EVA/ Rosin (E/R) samples, the log number of survival of the applied strains increased. On the other hand, the tested strains incubated with EVA/ Rosin/Cinn [E/R/(C 5%)], EVA/Rosin/Ag [E/R/ Ag 5%], and EVA/Rosin/Cinn/Ag [(E/R/C/Ag 5%)] suffered an increasing shortage in the log number of survivors by 2 log and 3 log cycles, respectively, for all the tested strains at the end of contact time. Additionally, it appeared from the results that *P. aeruginosa* was more resistant to the compounds under evaluation than *S. aureus*. Gram +ve bacteria have been found to be more sensitive to antimicrobial treatments than Gram -ve bacteria; according to El- Astal *et al.* (2005),[34] this may be due to the Gram +ve cell wall is less complex. Furthermore, Gram-negative species are thought to have an outer membrane covering the cell wall, and they are less susceptible to the effects of antibacterial agents.

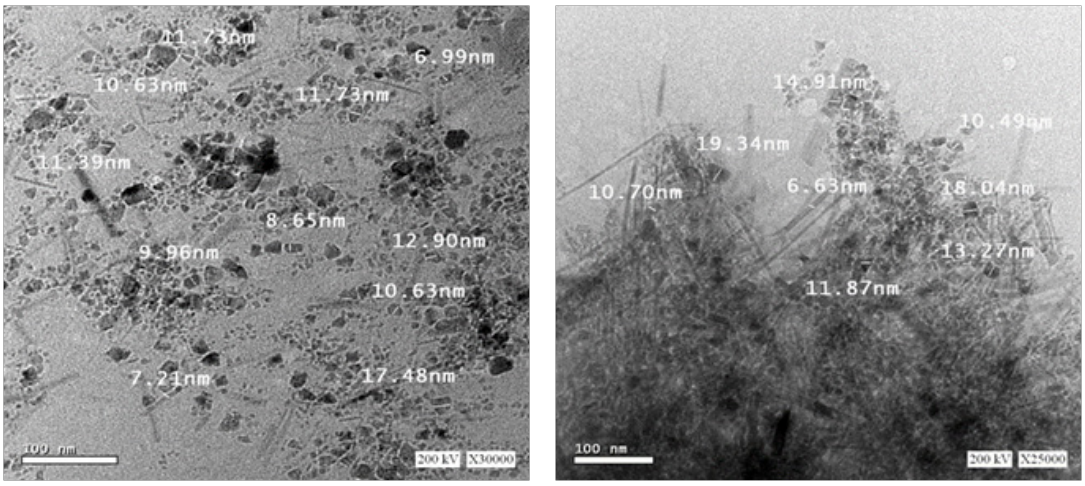

Fig. 5.TEM images of a) pure Ag NPs and b) Cinn/AgNPs nanoparticles.

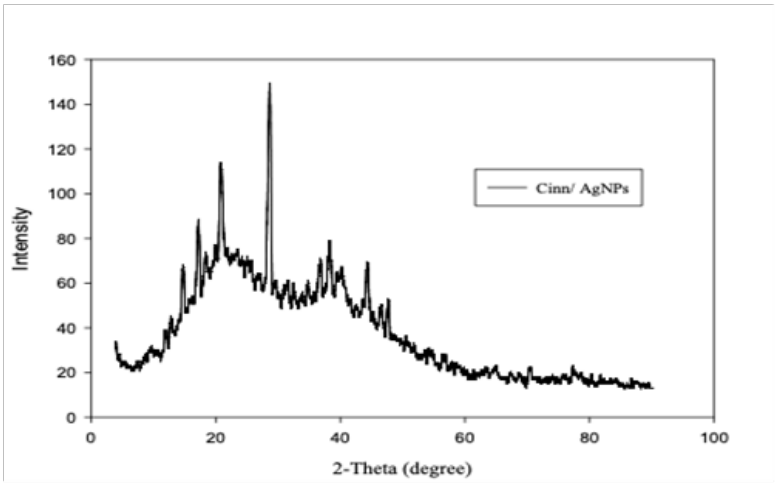

Fig. 6. XRD patterns of Cinn/ Ag NPs nanoparticls.

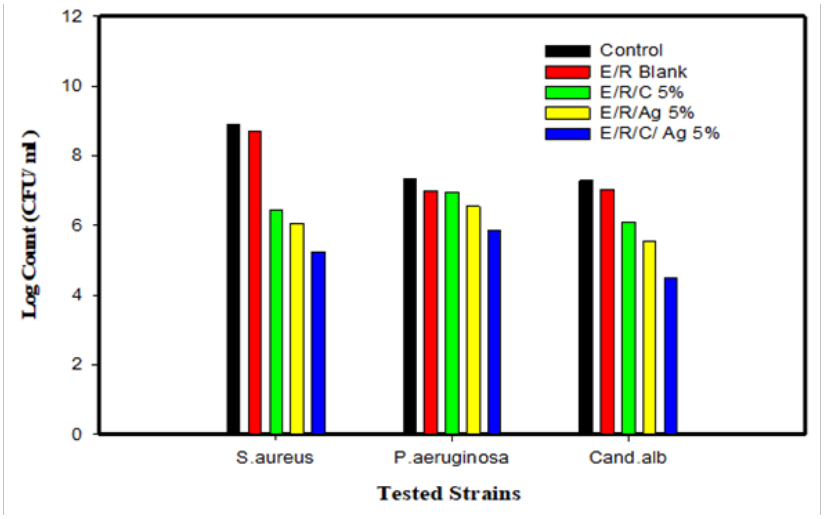

Fig. 7. Antimicrobial activity of the tested compounds on the different microbial strains.

The efficient antimicrobial activity of the EVA/ Rosin/(Cinn 5%), EVA/Rosin/(Ag NPs 5%) and EVA/Rosin/ (Cinn/ Ag NPs) 5%) compounds may be attributed to the constituents, which are mainly cinammic acid and silver nanoparticles. More inactivated cells were produced by the application of the (EVA/Rosin/ (Cinn/ Ag NPs) 5 %) treatment than by either of the individual treatments (EVA/ Rosin/Cinn 5%) or (EVA/Rosin/ Ag NPs 5%). These findings suggest that the combination use of silver nanoparticles with cinnamic acid produced a positive synergistic impact. This strategy may also improve bactericidal effectiveness and decrease the chances that pathogens may re-grow. Inorganic nanoparticles (Ag NPs) have different forms, a high surface-to-volume ratio, and nanoscale size. Because of this, they are able to interact and combine with some pathogenic microbes, including fungus, yeast, and bacteria[35, 36]. According to Singh et al. (2017)[37] and AbdElkodous et al. (2019)[38]. Ag NPs have exceptional properties that make them effective in a variety of biomedical applications and reduce the effectiveness of conventional antibiotics by making some bacteria more resistant to them. This reduces the probability that these medications will be effective.

Zhang et al. (2019),39 mentioned that cinnamic acid was expected to be a promising agent for inactivating *Stenotrophomonas maltophilia,* and the main antibacterial mechanism of cinnamic acid was related to membrane damage, produced by the loss of cell membrane integrity and modification of cell morphology.

Using the Congo red agar technique, the tested strains were assessed for exopolysacharide production both before and after treatment with the four synthesized compounds. According to the observations shown in Fig. (8), all untreated strains (control) produced exopolysaccharides in significant amounts. This is demonstrated by the formation of dark, dry, crystalline colonies on Congo Red Agar plates. The findings also showed that the E/R treatment was insufficient to prevent the formation of a slime layer. However, treatment with the other three compounds, EVA/Rosin/Cinn 5%, EVA/Rosin/ AgNPs 5% and EVA/Rosin/ (Cinn/AgNPs) 5%, was effective in reducing slime formation to weak amounts (pink or white colonies).

According to Hola et al. (2006)[40] and Menge et al. (2013)[41]*, P.aeruginosa* is capable of producing a significant amount of slime-like substance, which the bacterial cell uses to improve adherence to the plastic surface of the catheter. Adhesion and biofilm production on implanted medical devices are significant contributors to the pathogenesis of all microorganisms and significantly increase patient morbidity and mortality.

Antibiofilm Potential of the Synthesized Compounds

A biological or non-biological surface covered in microbial aggregation is called a biofilm. The production of biofilms is a serious problem in the food, medical, and marine industries and can have adverse effects on both human health and the economy. Antibiotics and sanitizers are ineffective against the complex microbial population found in biofilms (Sadekuzzaman et al., 2015).[42] The tube method was used to assess the biofilm produced by *S. aureus, P. aeruginosa*, and *C. albicans* in the presence and absence of the tested compounds. It was indicated by the results that *S. aureus* inoculated in test tubes in the absence and presence of (E/R) and (E/R C 5%) demonstrated a ring completely attached to the test tube's wall and bottom and appeared as a blue ring due to crystal violet (CV) staining. On the other hand, the test tubes containing *S. aureus* that were treated with (E/R/AgNPs 5% and E/R/C/ AgNPs 5%) showing a suppressed effect where the formation of bacterial rings was restricted. Furthermore, there was no blue color and only a pale blue color represented the adhering bacterial cells stained with CV. Similar findings were observed for the suppression of *P. aeruginosa* and *C. albicans* biofilms, as shown in Fig. (9).

The studied strains were tested for various compounds in the current experiment. Fig. (10) illustrates that all strains' capability to form biofilm was reduced when (E/R/C5 % and E/R/ AgNPs 5%) used in comparison to the control and blank (E/R) groups. Furthermore, it was determined that E/R/C/AgNPs 5% was the most effective compound that significantly inhibited the formation of biofilms. Fortunately, *P. aeruginosa* was adversely impacted by the E/R/C/AgNPs 5%, which resulted in a change from a strong (O.D. = 0.960) to a weak (O.D. = 0.223) producer. A similar response was seen for *C. albicans* and *S. aureus*, which changed from being strong (O.D. = 0.760) to weak producers (O.D. = 0.217) and from being strong (O.D.= 0.625) to being weak (O.D.= 0.209), respectively. Silver nanoparticles (AgNPs) were tested for their antibiofilm efficacy against *P. aeruginosa* and *S. epidermidis* strains by (Kalishwaralal *et al*. 2010),[43] the authors found that the treatment with AgNPs inhibited biofilm formation without affecting bacterial viability. Similarly, Mohanty *et al.* (2012)[44] reported that AgNPs have dose-dependent efficacy against *S. aureus* and *P. aeruginosa* biofilm.

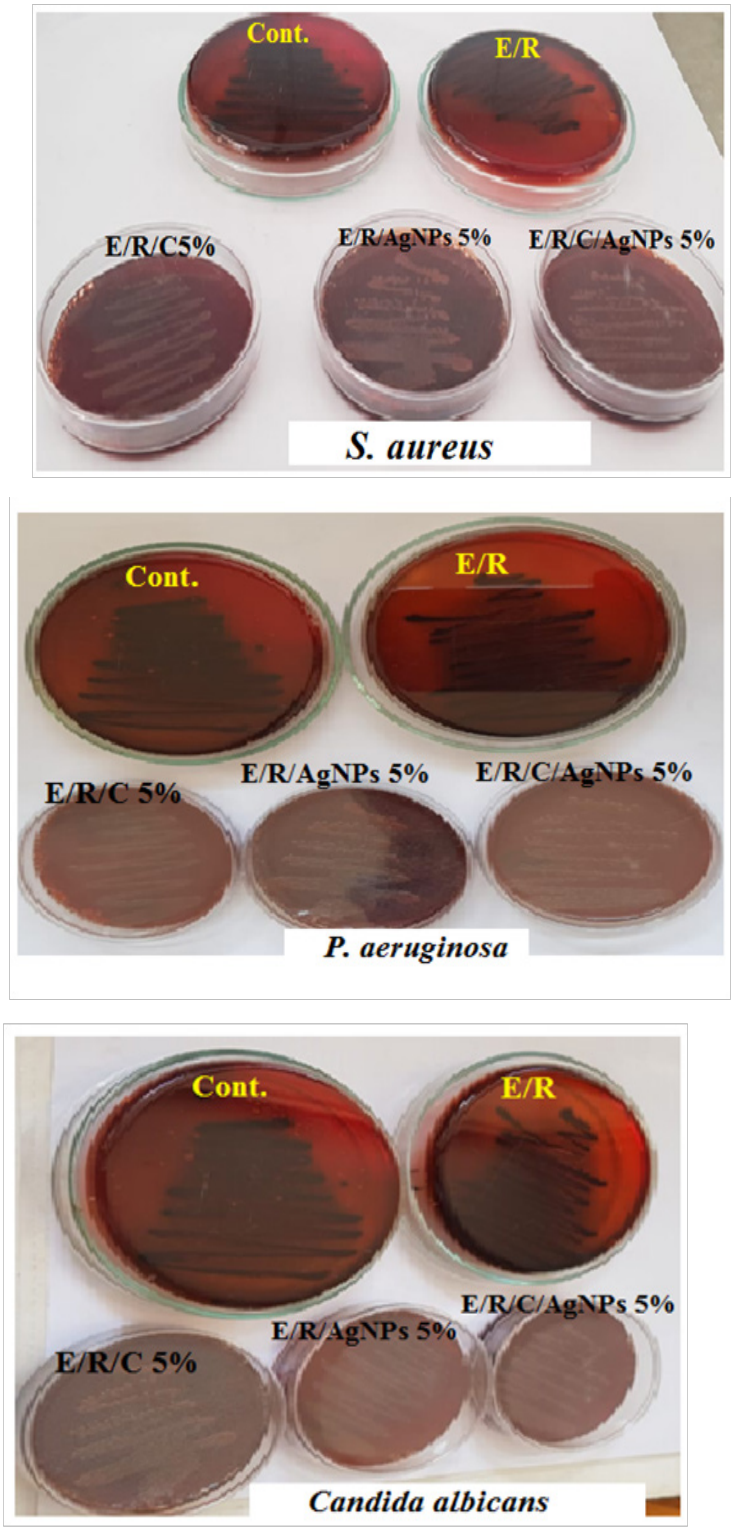

Fig. 8. Slime production for the tested strains before and after treatment with the tested compoundsThe black color colonies indicate biofilm positive and the pink color colonies indicate biofilm negative.

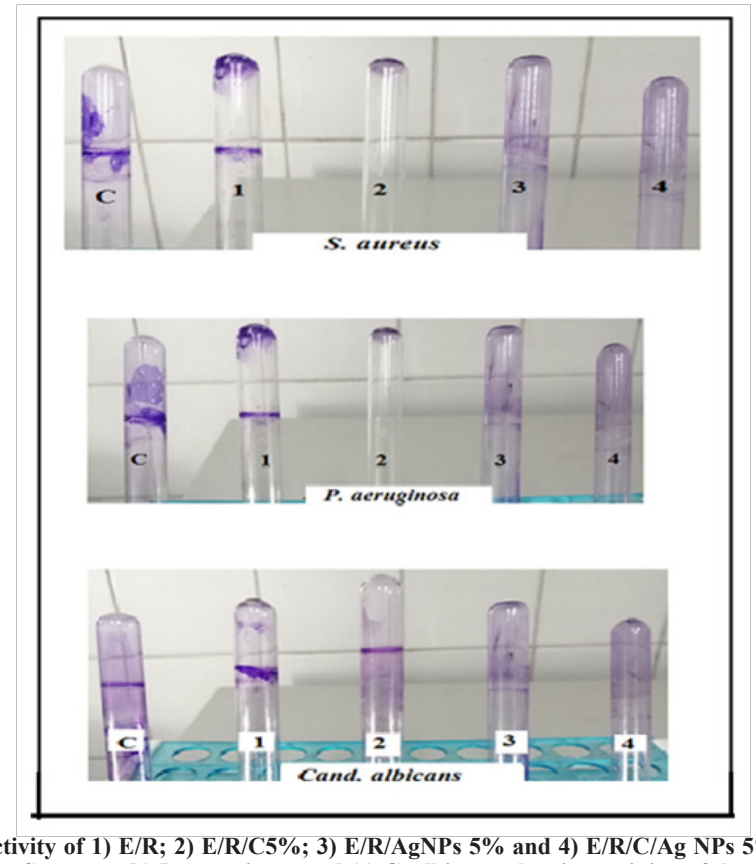

Fig. 9. Antibiofilm activity of 1) E/R; 2) E/R/C5%; 3) E/R/AgNPs 5% and 4) E/R/C/Ag NPs 5%; using the tube method against S. aureus (b) P. aeruginosa and (c) C. albicans, showing staining of the adherent bacterial and yeast cells with crystal violet; C control

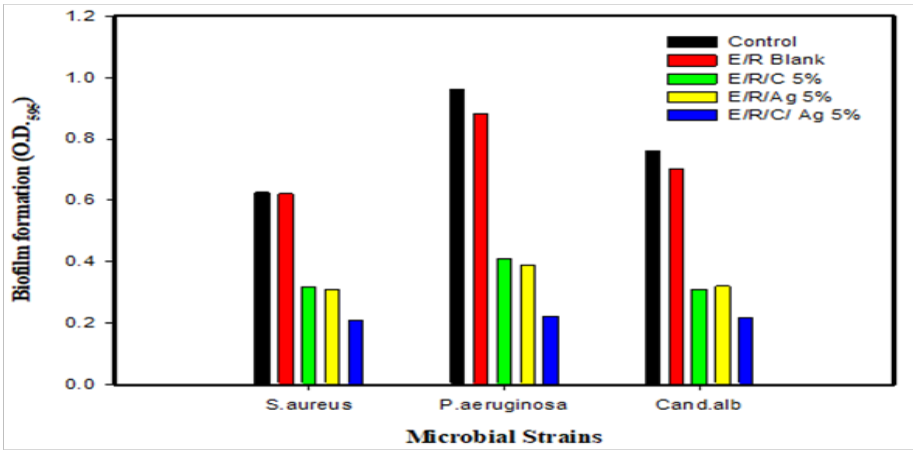

Fig. 10. Antibiofilm effect of the tested compounds on the microbial strains

Examination via scanning electron microscopy (SEM)

Microbial pathogens' cell surfaces may undergo morphological changes when they are exposed to antimicrobial treatments. In order to fully understand the influence of (E/R/C/ Ag NPs 5%) on the morphological and surface characteristics of the treated cells of *S. aureus* and *P. aeruginosa* in comparison to the control group, a SEM examination was performed. It was observed that the surfaces of the two strains' untreated cells were regular and smooth, whereas those of the treated cells were rougher and had irregular surfaces. Additionally, it is clear from the images that treated cells' morphologies differed noticeably from untreated ones in terms of their structural integrity and membrane permeability (Fig. 11).

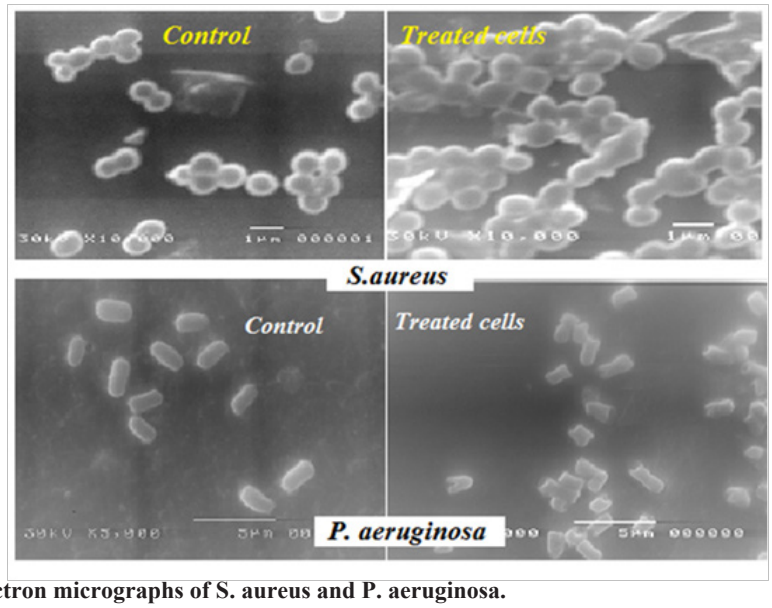

Fig. 11. Scanning electron micrographs of S. aureus and P. aeruginosa.

{Control and treated cells with E/R/C/AgNPs 5%}

Due to their size and large surface area, Ag NPs have strong antibacterial activity against both Gram-positive and Gram-negative bacteria. This activity is attributed to their ease of access to the nuclear content of bacteria. The silver cations that were released from Ag NPs were thought to be responsible for the bactericidal effect. These cations altered the structure of bacterial membranes, which in turn caused the bacteria's membrane permeability to increase and ultimately resulted in cell death. The release of Ag NPs from the synthesized compound (E/R/C/Ag NPs 5%) had initiated, and this was the beginning of the synthetic substance's potential antibacterial mechanism by adhesion at the outer surface of the *S. aureus* and *P. aeruginosa* cells (Bekhit et al., 2021).[45] According to El-Batal et al. (2020)[46], the released Ag NPs disrupted all intracellular structures, including plasmids, genetic materials, and other crucial organelles.

Conclusion

The current study aimed to prepare polymer blends of EVA / Rosin with different ratios (25/75, 50/50. 75/25) (wt/wt %) which have been prepared by solution casting technique followed by exposure to different doses (20, 50, 100 and 200 kGy) of gamma radiation. Moreover, the present study focused on the preparation and characterization of unirradiated and gamma-irradiated various compositions of (EVA/Rosin) blends and modified through incorporation of silver nanoparticles Ag NPs and cinnamic acid Cinn into EVA/Rosin. Careful examination of the IR spectrum of the EVA/Rosin (75/25) blend resulted in the combination and overlapping of the characteristic bands of both EVA and Rosin with a shift in wave number and a decrease in the intensity of some bands due to the strong interaction between EVA and Rosin. Verification that a gamma irradiation dose of 100 kGy makes cross-linking, crystallinity, and a chemical structure of the polymeric blend was done through XRD and FTIR analysis. Based on the results of the mechanical properties, the blend composition (75/25) of EVA/Rosin was chosen for further study because it exhibits the best Ts and Eb%. From SEM, it can be proven that the irradiation process increases the crosslinking degree of the blend, which modifies the interface of the blends and enhances the interaction of the two polymers. Additionally, from the evaluation of the antimicrobial and antibiofilm effect of four compounds (EVA / Rosin), (EVA / Rosin / Cinn), (EVA / Rosin / Ag NPs) and (EVA / Rosin / Cinn / Ag NPs) against some pathogenic strains, it can be concluded that the combined treatment of cinnamic acid and silver nanoparticles had a promising antimicrobial and antibiofilm potentiality against all the tested pathogens.

References

1. Bucek A, Brablec A, Kovacik D, et al. Glass bond adhesive strength improvement by DCSBD atmospheric-pressure plasma treatment. Int J Adhes Adhes 2017; 78: 1-3.

2. Norstrom E, Fogelstrom L, Nordqvist P, et al. Xylan – a green binder for wood adhesives. Eur Polym J 2015; 67: 483–493.

3. Nawaz, M., Baloch, M. K. & Rehman, W. Investigating the compatibility of polymers in common solvent. *Journal of the Chilean Chemical Society* **55**, 90–93 (2010).

4. Chandra S, Roy A, Jana M, Pahan K (2019) Cinnamic acid activates PPARα to stimulate Lysosomal biogenesis and lower Amyloid plaque pathology in an Alzheimer‘s disease mouse model. Neurobiol Dis 124:379–395.

5. Kırmusaoğlu S. 2016. Staphylococcal biofilms: Pathogenicity, mechanism and regulation of biofilm formation by quorum sensing system and antibiotic resistance mechanisms of biofilm embedded microorganisms. In: Dhanasekaran D, Thajuddin N, editors. Microbial Biofilms—Importance and Applications. Croatia: Intech; 2016. pp. 189-209. DOI: 10.5772/62943

6. B. Perito, E. Giorgetti, P. Marsili, and M. Muniz-Miranda, “Antibacterial activity of silver nanoparticles obtained by pulsed laser ablation in pure water and in chloride solution,” Beilstein J. Nanotechnol., vol. 7, no. 1, pp. 465–473, 2016.

7. M. Ratti et al., “Irradiation with visible light enhances the antibacterial toxicity of silver nanoparticles produced by laser ablation,” Appl. Phys. A Mater. Sci. Process., vol. 122, no. 4, pp. 1–7, 2016.

8. Y. G. Yuan, Q. L. Peng, and S. Gurunathan, “Effects of silver nanoparticles on multiple drug-resistant strains of Staphylococcus aureus and Pseudomonas aeruginosa from mastitis-infected goats: An alternative approach for antimicrobial therapy,” Int. J. Mol. Sci., vol. 18, no. 3, 2017.

9. P. Laux et al., “Nanomaterials: certain aspects of application, risk assessment and risk communication,” Arch. Toxicol., vol. 92, no. 1, pp. 121–141, 2018.

10. J. Natsuki, T. Natsuki, and Y. Hashimoto, “A Review of Silver Nanoparticles: Synthesis Methods, Properties and Applications,” Int. J. Mater. Sci. Appl., vol. 4, no. 5, p. 325, 2015, doi: 10.11648/j.ijmsa.20150405.17.

11. R. A. Ismail, G. M. Sulaiman, M. H. Mohsin, and A. H. Saadoon, “Preparation of silver iodide nanoparticles using laser ablation in liquid for antibacterial applications,” IET Nanobiotechnology, vol. 12, no. 6, pp. 781–786, 2018.

12. R. M. Kumar, B. L. Rao, S. Asha, B. Narayana, K. Byrappa, and Y. Wang, “Gamma radiation assisted biosynthesis of silver nanoparticles and their characterization,” no. January, 2015.

13. M. Scuderi et al., “Nanoscale Study of the Tarnishing Process in Electron Beam Lithography-Fabricated Silver Nanoparticles for Plasmonic Applications,” J. Phys. Chem. C, vol. 120, no. 42, pp. 24314–24323, 2016.

14. M. Parveen, F. Ahmad, A. M. Malla, and S. Azaz, “Microwave-assisted green synthesis of silver nanoparticles from Fraxinus excelsior leaf extract and its antioxidant assay,” Appl. Nanosci., vol. 6, no. 2, pp. 267–276, 2016.

15. E. M. Halawani, “Rapid Biosynthesis Method and Characterization of Silver Nanoparticles Using Zizyphus spina Christi Leaf Extract and Their Antibacterial Efficacy in Therapeutic Application, J. Biomater. Nanobiotechnol., vol. 08, no. 01, pp. 22–35, 2017.

16. M. Ndikau, N. M. Noah, D. M. Andala, and E. Masika, “ Green Synthesis and Characterization of Silver Nanoparticles Using Citrullus lanatus Fruit Rind Extract ,” Int. J. Anal. Chem., vol. 2017, pp. 1–9, 2017, doi: 10.1155/2017/8108504. 19 Journal of Research in Nanoscience and Nanotechnology Volume 3, Issue 1 (2021) 53-75 72.

17. J. K. Patra and K. H. Baek, “Green Nanobiotechnology: Factors Affecting Synthesis and Characterization Techniques,” J. Nanomater., vol. 2014, 2014.

18. D. M. Clifford, C. E. Castano, and J. V. Rojas, “Supported transition metal nanomaterials: Nanocomposites synthesized by ionizing radiation,” Radiat. Phys. Chem., vol. 132, no. October 2016, pp. 52–64, 2017, doi: 10.1016/j.radphyschem.2016.12.001.

19. M. Ghorab, A. El-Batal, A. Hanora, and F. Mosalam, “Incorporation of Silver Nanoparticles with Natural Polymers Using Biotechnological and Gamma Irradiation Processes,” Br. Biotechnol. J., vol. 16, no. 1, pp. 1–25, 2016.

20. N. Misra, J. Biswal, V. P. Dhamgaye, G. S. Lodha, and S. Sabharwal, “A comparative study of gamma, electron beam, and synchrotron X-ray irradiation method for synthesis of silver nanoparticles in PVP,” Adv. Mater. Lett., vol. 4, no. 6, pp. 458–463, 2013, doi: 10.5185/amlett.2012.ib.114.

21. A. Abedini, A. A. A. Bakar, F. Larki, P. S. Menon, M. S. Islam, and S. Shaari, “Recent Advances

in Shape-Controlled Synthesis of Noble Metal Nanoparticles by Radiolysis Route," Nanoscale Res. Lett., vol. 11, no. 1, 2016

22. J. V. Garcia-Ramos, S. Sanchez-Cortes, A. Torreggiani, M. Tamba, Z. Jurasekova, and M. D'Angelantonio, "Fabrication of Ag nanoparticles by γ-irradiation: Application to surface-enhanced Raman spectroscopy of fungicides," Colloids Surfaces A Physicochem. Eng. Asp., vol. 339, no. 1–3, pp. 20 Journal of Research in Nanoscience and Nanotechnology Volume 3, Issue 1 (2021) 53-75 73 60–67, 2009, doi: 10.1016/j.colsurfa.2009.01.018.

23. A. Bera et al., "Gamma radiation synthesis of colloidal AgNPs for its potential application in antimicrobial fabrics," Radiat. Phys. Chem., vol. 115, pp. 62–67, 2015.

24. AATCC test method 100-2004: Antibacterial finishes on textile material : Assessment of. . Developed in 1961, AATCC Committee RA31.

25. Freeman J, Falkiner FR, Keane CT. (1989). New method for detecting slime production by coagulase negative staphylococci. Journal of Clinical Pathology. 1989;**42**:872-874.

26. Christensen, G. D. *et al.* Adherence of coagulase-negative staphylococci to plastic tissue culture plates: A quantitative model for the adherence of staphylococci to medical devices. *J Clin Microbiol* **22**, 996–1006 (1985).

27. N. Gupta, E. J. O'Loughlin and G. K. Sims (2019), in Microbial Metabolism of Xenobiotic Compounds, Springer, pp. 1–31.

28. Murat S and Mehmet C. A comparative study of gamma irradiation of poly (ethylene-co-vinyl acetate) and poly (ethylene-co-vinyl acetate)/ carbon black mixture. Mater Chem Phys 2005; 93: 154–158.

29. Wang L, Shi Y, Wang Y, et al. Composite catalyst of rosin carbon/Fe_3O_4: highly efficient counter electrode for dye-sensitized solar cells. Chem. Comm. 2014; 50: 1701–1703.

30. Wang Z, Yuan L and Tang C. Sustainable elastomers from renewable biomass. J. Chem. Res 2017; 50: 1762–1773.

31. Arora, P. K. *Microbial Metabolism of Xenobiotic Compounds*. *Microbial Metabolism of Xenobiotic Compounds* vol. 10 (2019).

32. Nirmalaa R, Woo-il B, Navamathavan R, et al. Influence of antimicrobial additives on the formation of rosin nanofibers via electrospinning. Colloid Surface B 2013; 104: 262–267

33. de Boer, J. & Pennings, A. J. The effect of pendant chains on the elasticity behaviour of polyethylene networks. *Colloid Polym. Sci.* **261**, 750–756 (1983).

34. El-Astal, Z.Y., A.E.R.A. Ashour and A.A.M. Kerrit, 2005. Antimicrobial activity of some medicinal plant extracts in Palestine. Pak. J.Med. Sci., 21(2): 187-193.

35. A.I. El-Batal, G.S. El-Sayyad, N.E. Al-Hazmi, M. Gobara,(2019). Antibiofilm and antimicrobial activities of silver boron nanoparticles synthesized by PVP polymer and gamma rays against urinary tract pathogens. J. Cluster Sci. **30**(4), 947–964 (2019)

36. M. Aravind, A. Ahmad, I. Ahmad, M. Amalanathan, K. Naseem, S.M.M. Mary, C. Parvathiraja, S. Hussain, T.S. Algarni, M. Pervaiz, (2021).Critical green routing synthesis of silver NPs using jasmine flower extract for biological activities and photocatalytical degradation of methylene blue. J. Environ. Chem. Eng. **9**(1), 104877 (2021)

37. Singh H, Du J, Yi TH (2017) Green and rapid synthesis of silver nanoparticles using Borago officinalis leaf extract: anticancer and antibacterial activities. Artif Cells Nanomed Biotechnol 45:1310– 1316.

38. M. Abd Elkodous, G.S. El-Sayyad, A.M. Mia, I.Y. Abdelrahman, F.M. Mosallam, M. Gobara, A.I. El-Batal, (2019). Fabrication of ultrapure anisotropic zinc oxide nanoparticles via simple and costeffective route: implications for UTI and EAC medications. Biol. Trace Elem. Res. **196**(1), 297–317.

39. Zhang, Y. *et al.* Structure-Dependent Inhibition of Stenotrophomonas maltophilia by Polyphenol and Its Impact on Cell Membrane. *Front Microbiol* **10**, 1–11 (2019).

40. Hola, V., Horakova, L., Ruzicka, F., Votava, M., and TeJkalova, R. (2006): Biofilm-positive microbes isolated from the environment of life- boxes for allogenic transplantations and from immune-compromised patients. Clinical Microbiology and Infection, 12 (SuppI.4): 838.

41. Meng, C., Qingsong, Y., and Hongmin, S. (2013): Novel strategies for the prevention and treatment of biofilm related infections. International Journal of Molecular Sciences, 14 (9): 18488-18501.

42. M. Sadekuzzaman, S. Yang, M.F.R. Mizan, and S.D. Ha (2015) Current and Recent Advanced Strategies

for Combating Biofilms, Comprehensive Reviews in Food Science and Food Safety, Vol. 14, 2015

43. Kalishwaralal K, BarathManiKanth S, Pandian K, Deepak V, Gurunathan S. (2010). Silver nanoparticles impede the biofilm formation by *Pseudomonas aeruginosa* and *Staphylococcus epidermidis*. Colloids Surf B Biointerfaces 79:340–4.

44. Mohanty S, Mishra S, Jena P, Jacob B, Sarkar B, Sonawane A. (2012). An investigation on the antibacterial, cytotoxic, and antibiofilm efficacy of starch-stabilized silver nanoparticles. Nanomedicine 8(6): 916–2.

45. Bekhit, M.; El-Sabbagh, H. S.; Mohamed, M. R.; El-Sayyad, S.G.; Sokary, R. (2021). Mechanical, Thermal and Antimicrobial Properties of LLDPE/ EVA/ MMT/Ag Nanocomposites Films Synthesized by Gamma Irradiation. Journal of Inorganic and Organometallic Polymers and Materials, 32, 631-645.

46. El-Batal, A.I., Abd Elkodous, M., El-Sayyad, G.S., Al- Hazmi, N.E., Gobara, M., Baraka, A.(2020). Gum Arabic polymer-stabilized and Gamma rays-assisted synthesis of bimetallic silver-gold nanoparticles: Powerful antimicrobial and antibiofilm activities against pathogenic microbes isolated from diabetic foot patients. Int. J. Biol. Macromol. **165**, 169–186.